



Montréal, Québec
May 29 to June 1, 2013 / 29 mai au 1 juin 2013

Effect of Edge Beams on the Shear Capacity of GFRP-Reinforced Concrete Exterior Beam-Column Joints

Shervin K.Ghomi¹, Mohamed Hasaballa² and Ehab El-Salakawy³

¹ M.Sc. Student, Dept. of Civil Eng., University of Manitoba, Winnipeg, MB, Canada

² PhD Candidate, Dept. of Civil Eng., University of Manitoba, Winnipeg, MB, Canada

³ Professor and CRC, Dept. of Civil Eng., University of Manitoba, Winnipeg, MB, Canada

Abstract: The non-corrodible glass fibre-reinforced polymer (GFRP) reinforcement is currently used in reinforced concrete (RC) infrastructure to avoid steel-corrosion problems. However, the behaviour of GFRP bars in tension-compression reversed cycles in RC frame structures has not been well investigated yet. Recently, very few studies have been conducted on the seismic behaviour of FRP-RC exterior beam-column joints; however, none studied the influence of the edge beams on the behaviour. Therefore, this study attempts to partially fulfill this gap by investigating the structural performance of GFRP-RC beam-column Joints with edge beams. In this paper, four full-scale exterior beam-column joints were constructed and tested under simulated seismic load conditions. Test specimens represent isolated beam-column joints from an end bay between the assumed points of contra-flexure located at the mid-height and mid-span of column and beam, respectively. Two test variables are discussed in this paper; the presence of the edge beams and the shear capacity of the joint under seismic loads. Test results are presented in terms of load-drift ratio relationship, ultimate capacity and mode of failure. Test results indicated that specimens with edge beams showed significant improvement in the behaviour in terms of lateral load-drift relationship and shear capacity of the joint.

1 INTRODUCTION

The research work done on the behaviour of concrete beam-column joints, reinforced with FRP bars, is still in its early stages with very few studies (Fukuyama et al. 1995; Said and Nehdi 2004; Mady et al. 2011; Hasaballa et al. 2011). These previous studies revealed that using FRP bars as flexural and shear reinforcement is feasible. However, the GFRP-RC specimens showed lack of energy dissipation when compared to their steel-RC counterparts. A viable solution to this issue may be the use of hybrid seismic resistant systems in which steel-RC shear walls can provide lateral load resistance and absorb the seismic energy while using GFRP-RC moment resisting frames as the main structural system to support gravity loads. The presence of steel-RC shear walls does not eliminate the need of the adjoining GFRP-RC frame members to share part of the seismic loads and lateral drifts through their seismically-induced deformations. Accordingly, GFRP-RC moment resisting frames should be properly designed and detailed. Moreover, there is still a lack of research on the key parameters that are known to affect the behaviour of beam-column joints in FRP-RC structures, such as: 1) anchorage type of beam longitudinal reinforcements, 2) column-to-beam flexural strength ratio, 3) shear stress in joint, 4) confinement reinforcement in joint, 5) concrete strength, 6) presence of axial load on the column, and 7) geometry of joint with respect to the attached structural members. This lack of research limits the use of FRP reinforcement in new concrete construction. For example, Clause 12.7 in the CSA S806-12 code (CSA 2012) allows the use of FRP transverse reinforcement in moment resisting frame members subjected to significant axial load. It also specifies the amount and spacing of FRP stirrups required for confinement of

such members. However, due to lack of research and experimental data in this field, the CSA S806-12 code (CSA 2012) doesn't specify a safe level of shear capacity of the beam-column joint under seismic loads when the joint is confined according to this clause.

Only few researches have been done on the shear capacity of exterior beam-column joints fulfilling Clause 12.7 of CSA S806 (CSA 2002 & 2012). These researches have considered the behaviour of the joints without edge beams even though it is very common to have such edge beams in real structures as shown in Figure 1. Therefore, one of the main objectives of this in-progress study is to investigate the influence of the presence of the edge beams on the shear capacity of GFRP-RC beam-column joints to partially fill this gap in the CSA S806-12.

Also, due to the discontinuity nature of the end-bay beams, exterior beam-column joints exhibit anchorage loss of beam longitudinal reinforcement embedded in the joint when sufficient development length is not provided. In most cases, the development length required for longitudinal beam reinforcement may exceed the column depth in that direction. In steel-RC frames, standard 90-degree hooks are commonly used to anchor beam longitudinal bars within the joint. However, the drawback of using this approach with FRP-RC beam-column joints is the tensile strength reduction of FRP bent bars due to fibre bending. Therefore, using FRP straight headed bars seem to be a viable solution to overcome this problem. On the other hand, the performance of GFRP headed-bars in beam-column joints subjected to seismic loads has not been investigated yet. Therefore, it deems necessary to evaluate the performance of beam-column joints reinforced with GFRP-headed bars as well.

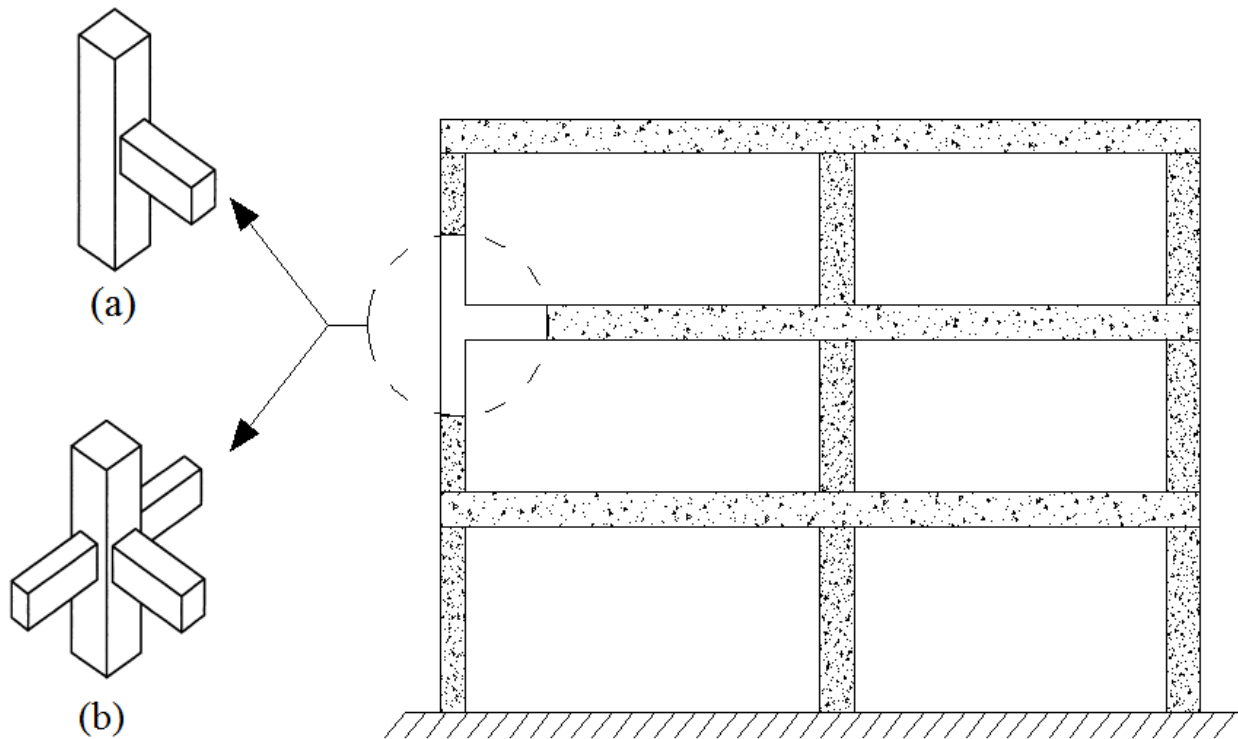


Figure 1: Exterior beam-column joints, (a) No edges beams, (b) Edge beam on two opposite sides

2 EXPERIMENTAL PROGRAM

2.1 Test Specimens

This study is part of an extensive experimental program started in 2007 and currently in-progress in the McQuade Heavy Structural Laboratory at the University of Manitoba to investigate the performance of GFRP-RC frames subjected to seismic loading. This experimental program includes design, construction, and testing of twenty full-scale test prototypes with and without edge beams. Test specimens represent isolated beam-column joints from an end bay between the assumed points of contra-flexure located at the mid-height and mid-span of the column and the beam, respectively, as shown previously in Figure 1. In this paper, the preliminary results of only four specimens will be presented and discussed. Specimens presented in this paper are divided into two series. Series (I) has two specimens, I-0.8 and I-1.0, with no edge beams attached to the joint and Series (II) has two specimens, II-0.8 and II-1.0, where the joint is confined with edge beams in two opposite sides as shown in Figure 2. Specimens are named in a way that the first character identifies the Series and the second character identifies the shear stress level in the joint in terms of $\sqrt{f'_c}$; for example, specimen II-0.8 belongs to Series II and the shear stress in the joint is equal to $0.8\sqrt{f'_c}$; where f'_c is the concrete compressive strength. All specimens are reinforced with GFRP headed bars and stirrups and they also have the same concrete dimensions, as shown in Figure 2, except for the presence of the edge beams. Specimens are designed to follow the strong column-weak beam concept with a column-to-beam flexural strength ratio larger than 1.0. The deformable concrete crushing failure in the beam section near the joint was considered to be achieved by providing a longitudinal reinforcement ratio, in the beam, larger than the balanced one. At the time when this program started, the spacing and amount of GFRP stirrups were calculated based on the CSA S806-02 code (CSA 2002), Clause 12.7. Table 1 shows the design characteristics of each specimen based on the concrete strength on the day of testing.

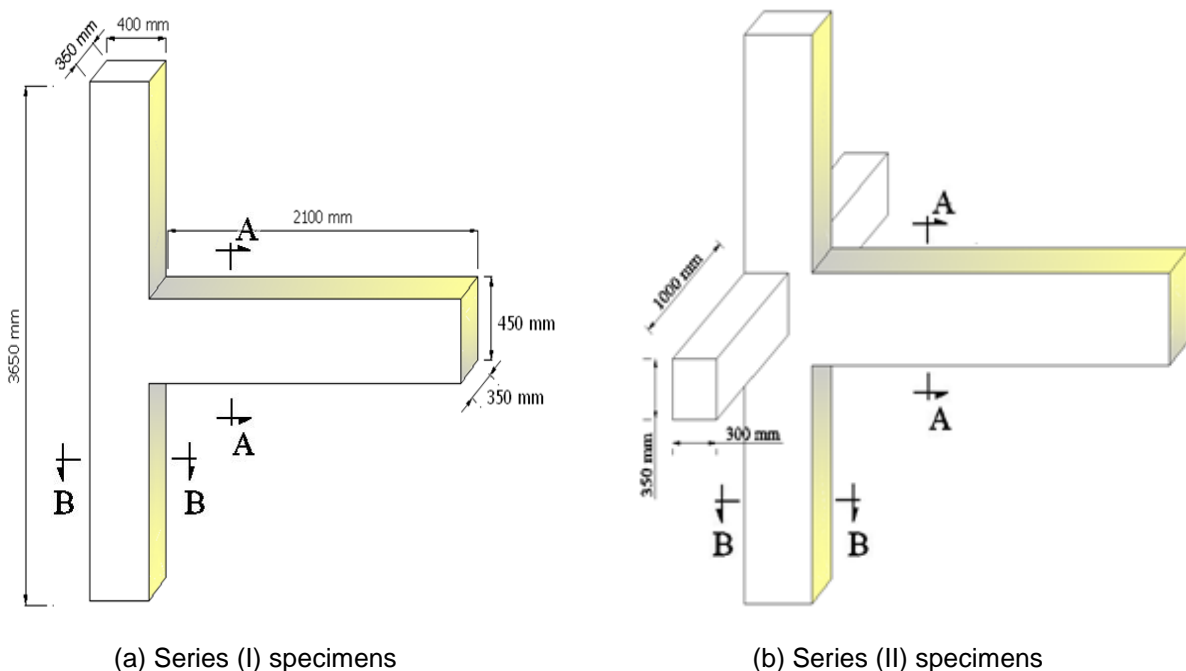


Figure 2: Dimensions and reinforcement details of test specimens

	Specimen I-1.0	Specimen I-0.8
	Specimen II-1.0	Specimen II-0.8
Sec A-A		
Sec B-B		

(c) Reinforcement details



(d) GFRP Headed-bars

Figure 2: Dimensions and reinforcement details of test specimens (Cont.)

Table 1 - Design characteristics of tested specimens based on concrete strength on the day of testing

	Specimen ID	I-0.8	I-1.0	II-0.8	II-1.0
Beam	End Anchorage	Headed Bars			
	Calculated Bar stress (MPa)	728	566	836	650
	$\rho_{frp} / \rho_{bal}^*$	2.09	3.33	1.63	2.59
	Flexural capacity (kN.m)	262	304	307	359
Overall	Transverse reinforcement	GFRP stirrups			
	Flexural strength ratio	1.53	1.4	1.39	1.19
	Joint shear stress (MPa)	4.66	5.84	5.37	6.69
	Concrete Strength (MPa)	$0.82\sqrt{f'_c}$	$0.98\sqrt{f'_c}$	$0.81\sqrt{f'_c}$	$0.97\sqrt{f'_c}$
	Concrete Strength (MPa)	32.6	35.6	44.4	47.8

* ρ_{frp} / ρ_{bal} is the ratio between the provided reinforcement ratio to the balanced reinforcement ratio.

2.2 Material properties

Test specimens were constructed using normal-weight, ready-mixed concrete with a targeted concrete compressive strength of 35 MPa and a maximum aggregate size of 20 mm. The obtained average concrete compressive strength on the day of testing was in the range of 33 to 48 MPa as shown in Table 1. The GFRP bars used in this study (Schoeck Canada 2011) had a deformed surface (ribs), as shown in Figure 2, and a high modulus of elasticity. Table 2 lists the mechanical properties of the GFRP reinforcing bars as measured according to CSA S806-02 (CSA 2002) standard tests.

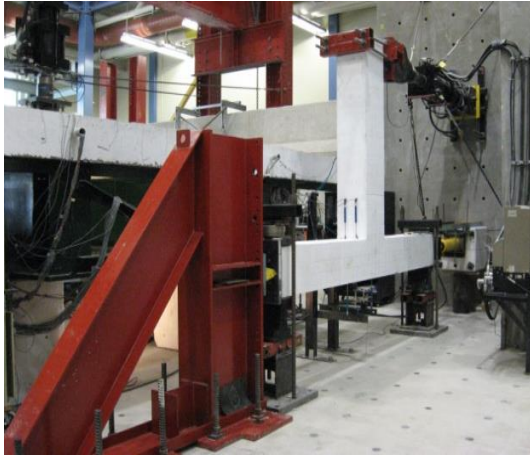
Table 2 - Properties of GFRP bars

Bar configuration	Bar Diameter (mm)	Tensile Elastic Modulus (GPa)	Ultimate Tensile Strength (MPa)	Ultimate Tensile Strain (%)
Stirrups	12	50	750	1.50
Headed bars	16	60	1100	1.83

2.3 Test set-up

All specimens are tested while the column is lying horizontally and subjected to constant axial load by means of a horizontal 1000 kN capacity hydraulic jack. The beam, on the other hand, is positioned vertically and a fully dynamic actuator, 1000 kN capacity and 500 mm stroke, applies the reversal cyclic loading to the beam tip. The actuator is positioned horizontally against a rigid RC reaction wall as shown in Figure 3.

The two ends of the column are restrained against both vertical and horizontal displacements meanwhile their rotations are allowed (hinged boundary conditions) to simulate the assumed contra-flexure points. A stiff steel frame is pre-stressed to the strong floor to carry the horizontal column's reaction.



(a) Series (I) specimens



(b) Series (II) specimens

Figure 3: Test set-up

2.4 Seismic Loading Scheme and Test Procedure

During testing, the column and transverse beams were loaded under a constant load while the fully dynamic actuator is utilized to apply the reversed quasi-static cyclic loading to the tip of the beam following the loading scheme shown in Figure 4. The magnitude of the axial load on the column is kept constant at a level equal to approximately 15% of the maximum concentric axial load capacity of the column. For Series (II) specimens, the tips of the edge beams are loaded with a constant magnitude and direction load to simulate the service condition loading. These loads were applied before starting the cyclic loading and maintained constant during the test.

The cyclic loading scheme is applied in a displacement-controlled mode that is simply consisted of applying variable amplitudes of displacement cycles (represents increasing drift ratio) in several steps (ACI 2005; Ghobarah and El-Amoury 2005). Each step consists of three identical (constant amplitude) displacement cycles in order to insure stable formation of cracking pattern. After each seismic loading step, one loading cycle with the peak load equal to service load condition is applied under a load-controlled mode in order to assess stiffness degradation of the test specimen due to applying the prescribed seismic loading scheme, if any. It should be noted that the service load condition is that corresponding to 25.0% of the GFRP ultimate tensile strain of the beam longitudinal reinforcement.

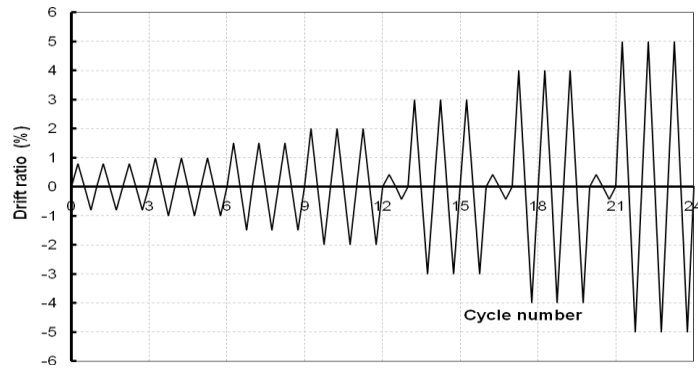


Figure 4: Seismic loading scheme

3 TEST RESULTS AND DISCUSSION

3.1 Load-Lateral Drift Response

Plots of the hysteresis diagrams represent the relationship between the applied lateral load and the drift ratio of the beam tip (Fig. 5). The drift ratio was calculated as the ratio between the horizontal displacement of the beam tip to the distance between the point of load application and the column centreline (i.e. 2200 mm). Figure 5(a) shows that specimen I-0.8 demonstrated stable linear-elastic response up to a drift ratio of 4.0%. At 5.0% drift ratio the specimen started to show non-linear response when the specimen reached the design capacity on both loading directions. This can be attributed to the concrete deformation in the beam and the joint. On the other hand, specimen I-1.0 had the linear-elastic response up to 3.0% drift ratio, as shown in Figure 5(b), and the non-linear response started at the 4.0% drift ratio where the specimen hardly reached the design capacity on the positive side of loading and 90% of its design capacity in the negative side of loading. When comparing the two specimens together, it is clear that although the design flexural capacity of specimen I-1.0 was larger than that of specimen I-0.8, the later exhibited more drift ratio than the earlier. This can be attributed to the higher shear stresses in the joint in specimen I-1.0 which accelerated the failure of the specimen as will be seen in the discussion of the mode of failure.

Contrary to Series (I), both specimens in Series (II) not only reached the design capacity but exceeded it. Specimen II-0.8, as shown in Figure 5(c), reached the design capacity at 4.0% drift ratio and exceeded it in the successive loading cycles up to 7.0% drift ratio in the positive side of loading. Failure of specimen II-0.8 occurred during the 7.0% drift ratio loading step on the negative direction of loading due to slippage of beam reinforcement. It is worth mentioning that the loads on the edge beams resulted in compression on one side of the joint (positive loading direction) and tension on the other side (negative loading direction). Slippage of beam bars occurred in this negative loading direction side.

A comparison between Series (I) specimens and their counterparts in Series (II) shows that the presence of the edge beams improved the hysteretic behaviour of Series (II) specimens in forms of reducing degradation rate in the flexural resistance of the specimen while sustaining higher drift ratios. For example, as shown in Figures 5(b) and 5(d), specimens I-1.0 and II-1.0 reached the design capacity at the same drift ratio (4.0%); however, specimen II-1.0 exceeded the design capacity and showed higher deformability up to a drift ratio of 8.0% while specimen I-1.0 exhibited accelerated failure at only 5.0% drift ratio.

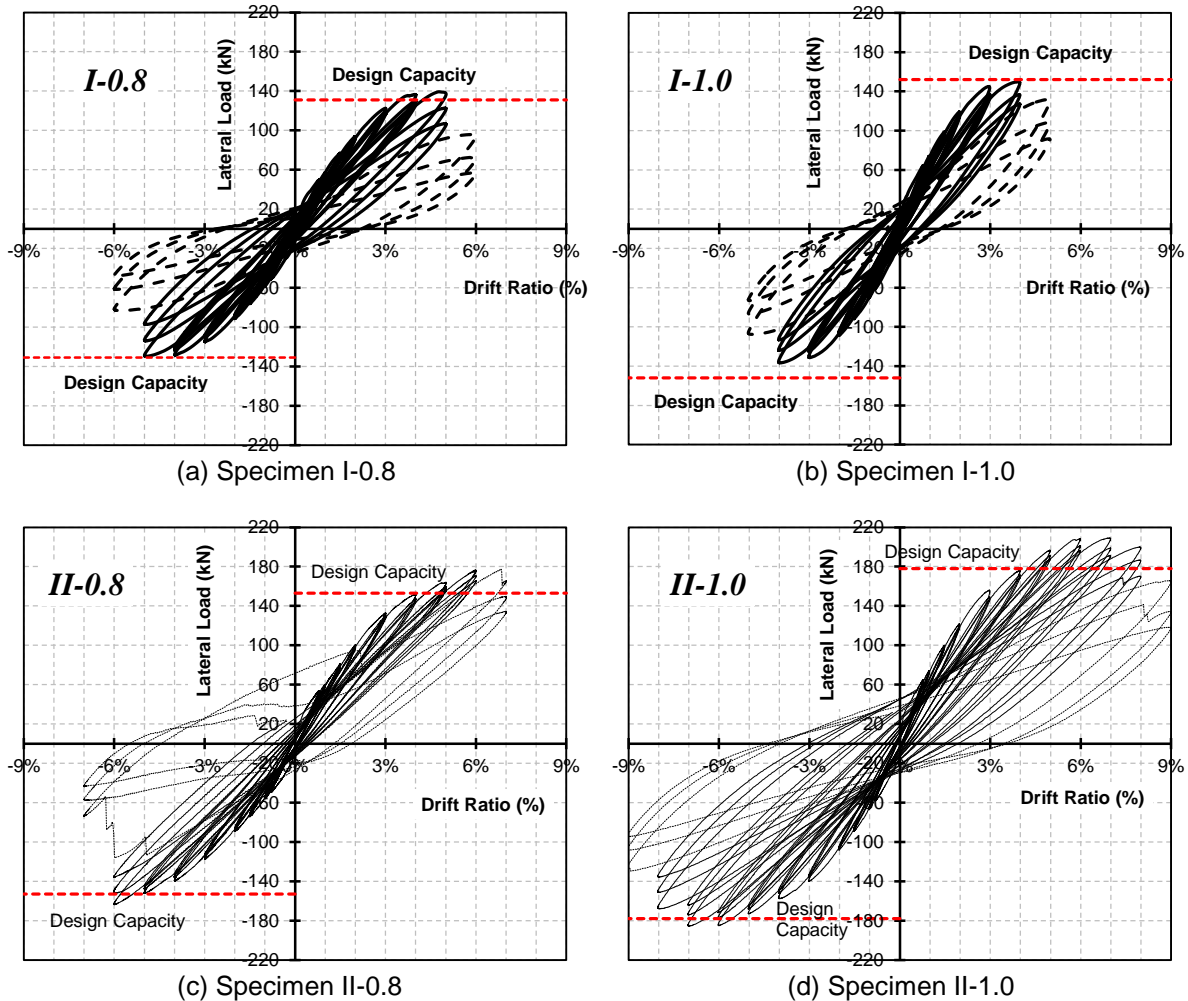


Figure 5: Load-lateral drift relationship

3.2 Mode of failure

Figure 6 shows the mode of failure of Series (I) specimens where the two specimens exhibited shear failure in the joint. Specimen I-0.8 developed a flexural resistance of approximately 278 kN.m at 4.0% drift ratio. This resistance was maintained until the first cycle of the 5.0% drift ratio loading step was reached. At this level, the shear stress developed in the joint reached 4.74 MPa (i.e. $0.84\sqrt{f'_c}$). By the end of the 5.0% drift ratio loading step, the specimen showed signs of failure such as concrete crushing in the beam and major diagonal shear cracks in the joint. The degradation of strength continued in the 6.0% drift ratio loading cycles until the joint failed in shear, as shown in Figure 6(a). Contrary, specimen I-1.0 developed a flexural resistance of approximately 300 kN.m at the first cycle of 4.0% drift ratio. At this level the specimen exhibited a shear stress in the joint equal to 5.85 MPa (i.e. $0.98\sqrt{f'_c}$) and couldn't maintain its capacity in the following cycles. Moreover, the specimen showed early signs of failure in the joint in the form of extensive diagonal shear cracks. Finally, at 5.0% drift ratio loading, the specimen exhibited complete diagonal shear failure in the joint, as shown in Figure 6(b). Regarding Series (II) specimens, both specimens exhibited virtual plastic hinges and flexural failure in the beam section adjacent to the column face due to gradual compression failure of concrete in the beam section as shown in Figures 7 and 8. However, specimen II-1.0 exhibited the joint shear failure simultaneously with the flexural failure in the beam section due to high shear stress level in the joint which reached 7.6 MPa (i.e. $1.10\sqrt{f'_c}$).



(a) Specimen I-0.8



(b) Specimen I-1.0

Figure 6: Failure of Series (I) specimens at the end of the test



(a) General view of the beam



(b) Joint surface from the bottom of the specimen

Figure 7: Failure of specimen II-0.8



(a) General view of the beam



(b) Joint surface from the bottom of the specimen

Figure 8: Failure of specimen II-1.0

4 CONCLUSIONS

Based on the test results, the following conclusions can be derived:

1. In specimen I-1.0 with no edge beam, the high joint shear stresses, $1.0\sqrt{f'_c}$, significantly affected the capability of the specimen to undergo larger drift ratio and to maintain its flexural capacity. Also, this high shear stress accelerated the failure of the joint. Contrary, the counterpart specimen in series II, specimen II-1.0, sustained higher value of shear stress in the joint and maintained its flexural capacity up to 8.0% drift ratio as a result of the joint confinement provided by the presence of the edge beams.
2. Specimen I-0.8 exhibited failure due to concrete crushing in the beam section associated with a diagonal shear failure in the joint when the shear stress in the joint reached $0.82\sqrt{f'_c}$. While the counterpart specimen in Series II, specimen II-0.8, did not show any signs of shear failure in the joint because of the presence of the edge beam.

ACKNOWLEDGEMENT

The authors wish to express their gratitude for the financial support received from the Natural Science and Engineering Research Council of Canada (NSERC), through Discovery and Canada Research Chairs program. Also, the authors would like to acknowledge the equipment provided by Canada Foundation for innovation (CFI). The GFRP reinforcement, generously provided by Schoeck Canada Inc., is greatly appreciated.

REFERENCES

- ACI Committee 374. 2005. Acceptance Criteria for Moment Frames Based on Structural Testing and Commentary (ACI 374.1-05). *American Concrete Institute*, Farmington Hills, Mich.
- CSA. 2002. Design and construction of building components with fibre reinforced polymers, CAN/CSA-S806-02, *Canadian Standards Association*, Ontario, Canada.
- CSA. 2012. Design and construction of building components with fibre reinforced polymers, CAN/CSA-S806-12, *Canadian Standards Association*, Ontario, Canada.
- Fukuyama, H., Masuda, Y., Sonobe, Y. and Tanigaki, M. 1995. Structural Performances of Concrete Frame Reinforced with FRP Reinforcement. *Proceeding of the 2nd international RILEM Symposium, Non-Metallic (FRP) Reinforcement for Concrete Structures*, Ghent, Belgium, 1: 275-286.
- Ghobarah, A. and El-Amoury, T. 2005. Seismic Rehabilitation of Deficient Exterior Concrete Frame Joints. *Journal of Composites for Construction*, ASCE, 9: 408 - 416.
- Hasaballa, M.H., El-Ragaby, A. and El-Salakawy, E.F. 2011. Seismic performance of exterior beam-column joints reinforced with glass fibre reinforced polymer bars and stirrups. *Canadian Journal of Civil Engineering*, 38: 1092-1102.
- Mady, M., El-Ragaby, A. and El-Salakawy, E. 2011. Seismic Behavior of Beam-Column Joints Reinforced with GFRP Bars and Stirrups. *Journal of Composites for Construction*, ASCE, 15:875-886.
- Said, A.M. and Nehdi, M.L. 2004. Use of FRP for RC Frames in Seismic Zones: Part II. Performance of Steel-Free GFRP-Reinforced Beam-Column Joints. *Applied Composite Materials*, 11: 227-245.
- Schoeck Canada Inc. 2011. Schöck-ComBAR™, *Technical Information sheet*, Available from http://www.schoeck-canada.com/en_ca/download/combar--17#.